



## BASIC RESEARCH:

### Influence of Thermal Treatment on Fracture Due to Cyclic Fatigue of Rotary Files Influencia del tratamiento térmico en la fractura por fatiga cíclica de limas rotatorias

María Verónica Méndez-González DDS, MSc<sup>1</sup> <https://orcid.org/0000-0002-0620-6603>

Amaury Pozos-Guillén DDS, MSc, PhD<sup>2</sup> <https://orcid.org/0000-0003-2314-8465>

María Concepción Betanzos-Juárez DDS, MSc<sup>1</sup> <https://orcid.org/0000-0001-5699-0179>

Alejandra Izquierdo-Orozco DDS<sup>1</sup> <https://orcid.org/0009-0001-3333-1610>

César Gaitán-Fonseca MSc, PhD<sup>3</sup> <https://orcid.org/0000-0001-6452-2578>

Vladimir Alonso Escobar-Barrios MSc, PhD<sup>4</sup> <https://orcid.org/0000-0001-5414-696X>

Mariana Gutiérrez-Sánchez MSc, PhD<sup>1</sup> <https://orcid.org/0000-0002-7667-4648>

<sup>1</sup>Endodontics Postgraduate Program, Faculty of Dentistry, San Luis Potosí University, San Luis Potosí, S.L.P., México.

<sup>2</sup>Laboratory of Basic Sciences, Faculty of Dentistry, Autonomous San Luis Potosí University, San Luis Potosí, S.L.P., México.

<sup>3</sup>Biomedical Sciences Program, Universidad Autónoma de Zacatecas, Zacatecas, Mexico.

<sup>4</sup>Advanced Materials Division, Instituto Potosino de Investigación Científica y Tecnológica A.C, San Luis Potosí, Mexico.

Correspondence to: PhD.Mariana Gutierrez-Sánchez - [mariana.gutierrez@uaslp.mx](mailto:mariana.gutierrez@uaslp.mx)

Received: 28-I-2025

Accepted: 8-V-2025

**ABSTRACT:** The objective of this study aimed to assess the cyclic fatigue fracture of ZenFlex™, ProTaper Gold™, and HyFlex™. EDM rotary files in simulated curved canals, along with evaluating their physicochemical properties and thermal behavior. A total of 69 instruments from three different NiTi rotary file systems were utilized: ProTaper Gold™ (08/25), Hyflex™ EDM (08/25), and Zenflex™ (06/25). The analysis consisted of four phases: Phase 1 involved SEM observation to detect manufacturing defects; Phase 2 focused on cyclic fatigue-induced fracture in a curved canal with a 60° radius of curvature of 2 mm and a diameter of 1.5 mm; Phase 3 encompassed SEM observation of the fractured fragment and obtaining a fractographic study; Phase 4 included physicochemical characterization, such as equiatomic relationships by Inductively Coupled Plasma Optical Emission Spectroscopy (ICP-OES), phase transformation by DSC, crystalline structure by X-ray diffraction, and morphological analysis by SEM. Microcracks and defects were observed on cutting edges of ZenFlex™ and ProTaper Gold™ files. The mean cycles to fracture were  $2814.50 \pm 161.58$ ,  $2649.94 \pm 120.93$ , and  $1362.89 \pm 88.33$  for HyFlex™, ZenFlex™, and ProTaper Gold™, respectively. Moreover, different phase transition temperatures were noted, with ZenFlex™ in the austenite phase, ProTaper Gold™ in martensite, and HyFlex™ in the R phase at room temperature, as corroborated by X-ray diffraction. Additionally, a quasi-equimolar relationship was observed for the different systems, with ZenFlex™ exhibiting a reduced helical angle, followed by HyFlex™ and ProTaper Gold™. ZenFlex™ files demonstrated greater resistance to cyclic fatigue, which appeared to be attributed to their physicochemical properties, heat treatment, and design.

**KEYWORDS:** Austenite; Martensite; Cyclic fatigue; HyFlex™ EDM; ZenFlex™; Protaper Gold™.

**RESUMEN:** El objetivo de este estudio fue evaluar la fractura por fatiga cíclica de las limas rotatorias ZenFlex™, ProTaper Gold™ y HyFlex™ EDM en conductos curvos simulados, junto con sus propiedades fisicoquímicas y comportamiento térmico. Se utilizaron un total de 69 instrumentos de tres sistemas de limas rotatorias NiTi diferentes: ProTaper Gold™ (25/08), Hyflex™ EDM (25/08) y Zenflex™ (25/06). El análisis constó de cuatro fases: la fase 1 implicó la observación SEM para detectar defectos de fabricación; la fase 2 se centró en la fractura inducida por fatiga cíclica en un conducto curvo con un radio de curvatura de 60° de 2 mm y un diámetro de 1,5 mm; la fase 3 abarcó la observación SEM del fragmento fracturado y la obtención de un estudio fractográfico; la fase 4 incluyó la caracterización fisicoquímica, como las relaciones equiatómicas por Espectroscopia de plasma con acoplamiento inductivo (ICP-OES), la transformación de fase por DSC, la estructura cristalina por difracción de rayos X y el análisis morfológico por SEM. Se observaron microfisuras y defectos en los bordes de corte de las limas ZenFlex™ y ProTaper Gold™. Los ciclos medios hasta la fractura fueron  $2814,50 \pm 161,58$ ,  $2649,94 \pm 120,93$  y  $1362,89 \pm 88,33$  para HyFlex™ EDM, ZenFlex™ y ProTaper Gold™, respectivamente. Además, se observaron diferentes temperaturas de transición de fase, con ZenFlex™ en la fase austenítica, ProTaper Gold™ en martensita y HyFlex™ EDM en la fase R a temperatura ambiente, como lo corroboró la difracción de rayos X. Además, se observó una relación cuasi-equimolar para los diferentes sistemas, con ZenFlex™ exhibiendo un ángulo helicoidal reducido, seguido de HyFlex™ EDM y ProTaper Gold™. Las limas ZenFlex™ demostraron una mayor resistencia a la fatiga cíclica, que pareció atribuirse a sus propiedades fisicoquímicas, tratamiento térmico y diseño.

**PALABRAS CLAVE:** Austenita; Martensita; Fatiga cíclica; HyFlex™ EDM; ZenFlex™; ProTaper Gold™.

## INTRODUCTION

NiTi rotary instruments have revolutionized the field of endodontics due to their superplasticity and shape-memory properties, providing them with flexibility and resistance to fatigue. This allows them to navigate the intricate and varied geometries of root canals, ultimately reducing treatment time. These benefits extend to both practitioners and patients, as NiTi instruments also reduce the risk of canal transportation, preserve dentin, and decrease the likelihood of deformation or apical compression, especially in curved root canals (1-5).

The NiTi alloy typically comprises approximately 56% nickel and 44% titanium by weight, maintaining an equiatomic ratio of 1:1. Thermal treatments play an essential role in modifying

the thermoelastic martensitic transformation of the alloy, which can be induced either thermally or through tension. This transformation occurs in one step ( $B2 \leftrightarrow B19'$ ) or two steps ( $B2 \leftrightarrow R$  and  $R \leftrightarrow B19'$ ) (6). The austenite phase (B2) displays a body-centered cubic (BCC) crystalline structure, known for its elastic properties, contributing to its hardness and resistance.

Conversely, the martensite phase (B19') represents a low-temperature phase with a monoclinic crystalline structure, making it softer and more ductile compared to austenite, thereby demonstrating plastic behavior (6, 7). The R or rhombohedral phase represents a second-order transition, induced by tension in the crystalline network caused by Ti<sub>3</sub>Ni<sub>4</sub> precipitates, enhancing resistance to cyclic fatigue (8-10). However, even minor variations in composition, as small as 0.1%, can

lead to significant changes in transition temperatures and the mechanical properties of the alloy. Consequently, these variations can influence the behavior of the alloy during root canal procedures.

Despite its superelasticity, the risk of instrument fracture within the root canal remains a significant concern for endodontists. The incidence of fracture of rotary systems ranges from 0.09 to 5%, primarily attributed to cyclic fatigue. This phenomenon occurs when a NiTi endodontic instrument undergoes an excessive number of tension-compression cycles while rotating in a curved root canal, often unexpectedly. Fracture may lead to fragment remnants being retained within the canal, hindering cleaning and shaping procedures and potentially compromising treatment outcomes (11-15).

The objective of this study is to evaluate the cyclic fatigue of Protaper Gold™, Hyflex™ EDM, and Zenflex™ rotary systems while also assessing their physicochemical properties and thermal behavior.

## MATERIALS AND METHODS

This research has been conducted in full accordance with the World Medical Association Declaration of Helsinki and has been approved by the Research Ethics Committee of the Faculty of Stomatology, UASLP, with code: CEI-FE-041-021.

A total of 69 new instruments were utilized, comprising three distinct NiTi rotary file systems (n=23 each). Specifically, ProTaper Gold™ 25/.08 (Dentsply Tulsa Dental, Tulsa, OK, USA); Hyflex™ EDM 25/.08 (Coltene/Whaledent, Allstätten, Switzerland); and Zenflex™ 25/.06 (ZF; Kerr Corporation, Pomona, CA, USA).

## CYCLIC FATIGUE TEST

The cyclic fatigue was assessed using an Automatic Electronic Device (AED) (16) (refer to Figure 1). Each file was inserted to a depth of 18mm, and rotational movements were initiated following the manufacturer's instructions for each respective system: Protaper Gold™ (300 rpm and 3.1 Ncm), ZenFlex™ (500 rpm and 2 Ncm), and HyFlex™ EDM (400 rpm and 2.5 Ncm), until fracture occurred. The duration of each trial was recorded, and the resulting fragments were collected and measured for length using a digital vernier.

## DIFFERENTIAL SCANNING CALORIMETRY (DSC)

Phase transitions of the rotary instruments were analyzed using a TA-Instruments DSC Q2000 (TA Instruments, LLC, Waters, USA). Segments were cut from each rotating instrument, and 10 mg of the material was inside an aluminum pan (n=2/rotatory instruments by group). Subsequently, the samples were subjected to 2 heating and 2 cooling thermal cycles within a temperature range between -50 to 120°C, employing a rate of 5°C/min in a nitrogen atmosphere. Corresponding to the phase transitions were determined utilizing the specialized analysis software TA Universal Analysis (TA Instruments, LLC, Waters, USA).

## CHEMICAL ANALYSIS BY SPECTROSCOPY OF INDUCTIVELY COUPLED PLASMA (ICP-OES)

The chemical composition analysis of the instruments was conducted using ICP-OES. Segments weighing between 0.05 and 0.1mg were digested with a mixture consisting of 1.75 mL of 36.5-38% hydrochloric acid (HCl) (Macron, Fine Chemicals®, Radnor, PA, USA), 5.75 mL of 64.5-66.5% nitric acid (JT Baker), and 2 mL

of 48-51% hydrofluoric acid (HF) (Analytika®). These segments were placed in EasyPrep Plus CEM™ containers within a microwave (Mars 6 CEM™) programmed to undergo a 15-min ramp process with a power range of 900 to 1050 kW, followed by an isothermal process for 30 min at 210°C. Subsequently, the resulting solution was neutralized with 5 mL of 4% v/v boric acid (H3BO3) and diluted to a final volume of 50 mL with 2% v/v nitric acid. Finally, the samples were analyzed using ICP-OES at wavelengths of 308.802 nm for titanium (Ti) and 341.476 nm for nickel (Ni) using an iCAP 7400 Duo instrument (Thermo Scientific™, Waltham, MA, USA).

#### X-RAY DIFFRACTION

The crystalline phases of the instruments were analyzed using a PANalytical X'Pert PRO X-ray

diffractometer (PANalytical, Almelo, NL) operating at a wavelength of 1.54 Å with a 35 kV acceleration voltage and 30 mA current. The obtained diffraction patterns were then processed using the HighScore Plus software (PANalytical, Almelo, NL) to analyze signals and identify the crystalline phases present in the samples.

#### STATISTICAL ANALYSIS

The distribution of data was assessed using the Shapiro-Wilk test. A non-parametric Kruskal-Wallis analysis was employed to compare multiple groups, followed by Tukey's post hoc test for pairwise comparisons. All statistical tests were conducted at a significance level of 95% ( $\alpha=0.05$ ). Statistical analyses were conducted utilizing SAS JMP statistical software (SAS Institute Inc., Cary, NC, USA), version 16.

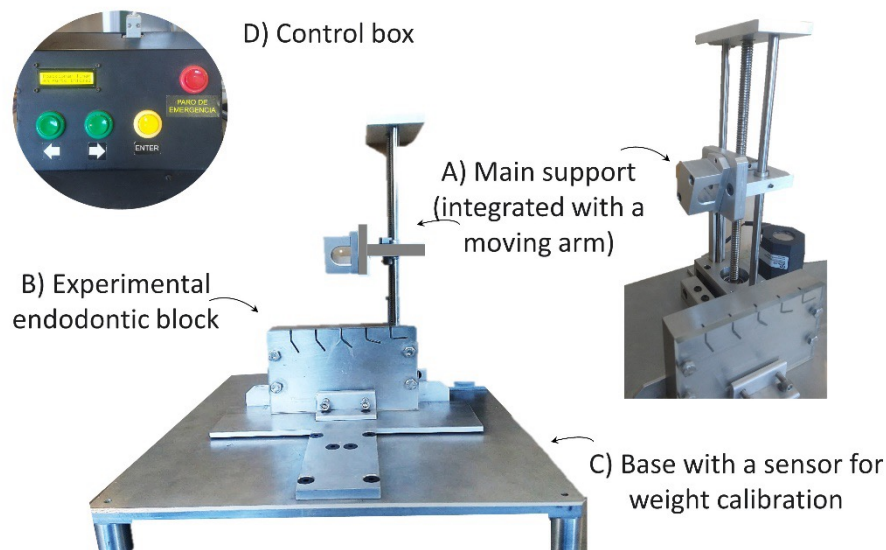


**Figure 1.** Automatic Electronic Device (AED). A) Main support, integrated with a mobile arm adaptable to the X-Smart plus motor (Dentsply Sirona); B) An experimental endodontic block, with artificial canals, C) Base with weight calibration sensor and D) Control box (16).

## RESULTS

Table 1 shows the mean values and standard deviations for fracture time (tF), number of cycles (NCF), and length of the fractured segment (FL). Statistically significant differences were observed among the three groups ( $p < 0.05$ , Kruskal-Wallis test). Post hoc analysis using the Tukey-Kramer method revealed significant differences ( $p < 0.05$ ) between ZenFlex™ and HyFlex™ EDM, ZenFlex™ and Protaper Gold™, as well as HyFlex™ EDM and Protaper Gold™ for each of the variables assessed. ZenFlex™ files showed the most significant resistance to cyclic fatigue, followed by HyFlex™ EDM and Protaper Gold™. Regarding fracture time, HyFlex™ EDM files showed the longest time to fracture, followed by the ZenFlex™ and Protaper Gold™ groups.

Figure 2 illustrates the SEM micrographs obtained before and after exposing the instruments to cyclic fatigue fracture. In Figure 2.A, the active portion of the ZenFlex™ instrument exhibits defects on the cutting edges, along with artifacts of organic residue and granules of excess material on the finished surface (indicated by arrows) (Figure 2.B). Similarly, defects are observed in the Protaper Gold™ experimental group, including circular, oval, and fused (coalescence) concavities in the non-cutting tip, as well as striations, micro-cracks on the cutting edge, and artifacts of organic residue and excess material granules on the finished surface (Figure 2.E). Manufacturing lines perpendicular to the file's longitudinal axis are also visible (Figure 2.F). For the HyFlex™ EDM experimental group, the micrograph shows the rectangular shape of the file's tip and defects on the lateral part, along with the characteristic surface finish corresponding to electrical discharge machining (Figure 2.I and Figure 2.J, respectively).

Subsequently, the fractographic study of the experimental groups after cyclic fatigue fracture is presented. In the cross-section of the ZenFlex™

experimental group, a triangular shape with peripheral cracks and crack propagation is evident (arrows) (Figure 2.C), along with patterns of cones and craters characteristic of cyclic fatigue failure (Figure 2.D). For the Protaper Gold™ experimental group, peripheral cracks and crack propagation are observed in the cross-section of the fracture (Figure 2.G), along with patterns of cones and craters and coalescence of micro-cavities (\*) in the approaches to the edge of the cross-section (Figure 2.H). Figure 2.K illustrates the trapezoidal cross-section of the HyFlex™ EDM file, showing the initiation of edge cracks (rounded area), peripheral indentations, and crack propagation (arrows), as well as patterns of cones and craters (delimited area), with crack propagation and coalescence of micro-cavities (\*) (Figure 2.L).

Thermal scans offer valuable insights into the phase transformations occurring in NiTi alloys as a function of temperature, as well as the energies involved in these transitions (Figure 3). Upon heating, endothermic peaks are observed, indicating the energy absorption required for the instrument to transition from the austenite phase to the martensite phase. For the Protaper Gold™ file, the onset of transformation occurred at a lower temperature compared to Zenflex™ and Hyflex™ EDM, commencing around 11.0, 30.26, and 38.4°C (As-austenitic onset), respectively, and concluding at 37.0, 60.5, and 61.4°C (Af-austenitic finish), respectively, with corresponding enthalpies of 3.42, 2.87, and 8.4 J/g. During the cooling process, the transformation from austenite to martensite was evident.

For the Hyflex™ EDM file, two exothermic peaks are observed, indicating a two-stage transformation process and the presence of an intermediate phase known as the R phase. The transformation begins at 65.3°C (Rs-R-phase onset) and concludes at 32.1°C (Rf-R-phase finish) with an enthalpy of 2.78 J/g, followed by a martensite phase starting at 5.6°C (Ms-martensitic onset)

and ending at  $-23.2^{\circ}\text{C}$  (Mf-martensitic finish) with  $3.54\text{ J/g}$ . Upon cooling, Zenflex<sup>TM</sup> and Protaper Gold<sup>TM</sup> exhibit a single-stage transition, starting at  $32.0$  and  $57.0^{\circ}\text{C}$  (Ms) and concluding at  $11.8$  and  $26.5^{\circ}\text{C}$  (Mf), with enthalpies of  $2.47$  and  $3.45\text{ J/g}$ , respectively.

The atomic ratio of Ni:Ti was determined using ICP-OES to be  $1.0:0.94$  for Zenflex<sup>TM</sup>,  $1.00:1.07$  for Protaper Gold<sup>TM</sup>, and  $1.00:1.06$  for Hyflex<sup>TM</sup> EDM. Statistical analysis revealed no significant difference in the nickel content ( $p=0.119$ ) or titanium content ( $p=0.079$ ) among the different rotary instruments. However, it is noteworthy that Zenflex<sup>TM</sup> exhibits a higher atomic content of nickel compared to titanium.

The design parameters of the rotary instruments were assessed by analyzing micrographs using the ImageJ program (Figure 4). In terms of the helical angle, Zenflex<sup>TM</sup> demonstrates a smaller angle ( $15.96\pm 1.21^{\circ}$ ) compared to Protaper Gold<sup>TM</sup> and Hyflex<sup>TM</sup> EDM, which exhibit more open angulations of  $19.77\pm 0.42^{\circ}$  and  $21.27\pm 0.73^{\circ}$ , respectively (Figure 4.A-C).

Regarding the type of point, all evaluated instruments feature a passive tip (Figure 4.G-I). The cross-sectional micrographs (Figure 4.J-L) reveal a negative cutting angle, with Protaper Gold<sup>TM</sup> and Hyflex<sup>TM</sup> exhibiting a triangular shape, while Zenflex<sup>TM</sup> displays a polyhedral section.

Figure 5 shows the X-ray diffraction (XRD) pattern of the rotary instrument files, providing insights into the phases present in the instruments at room temperature. In the case of Zenflex<sup>TM</sup>, the austenite phase (B2) was evident, characterized by an intense peak at  $42.614^{\circ}$  in  $2\theta$  associated with the (110) plane, along with two signals of better intensity around  $62$  and  $78^{\circ}$  in  $2\theta$  corresponding to the planes (200) and (211), respectively.

Contrastingly, the Hyflex<sup>TM</sup> EDM instrument exhibits a distinct pattern, featuring a double peak around  $42$  to  $43^{\circ}$  in  $2\theta$ , characteristic of the R phase. Furthermore, the XRD pattern of Protaper Gold<sup>TM</sup> demonstrates a broadening of the main peak, indicative of a coexistence of phases likely attributable to the temperature at which the analysis was conducted.

**Table 1.** Mean and standard deviation of time to fracture.

File	Time tF (s)	NCF	FL (mm)
ZenFlex <sup>TM</sup>	$336.33\pm 18.95$	$2814.50\pm 161.58$	$3.76\pm 0.37$
Protaper Gold <sup>TM</sup>	$272.58\pm 17.67$	$1362.89\pm 88.33$	$7.11\pm 0.25$
HyFlex EDM <sup>TM</sup>	$397.56\pm 18.15$	$2649.94\pm 120.93$	$6.58\pm 0.54$
Value p	$<0.05$	$<0.05$	$<0.05$

tF=time to fracture; NCF= number of cycles and FL length of the fractured fragments.

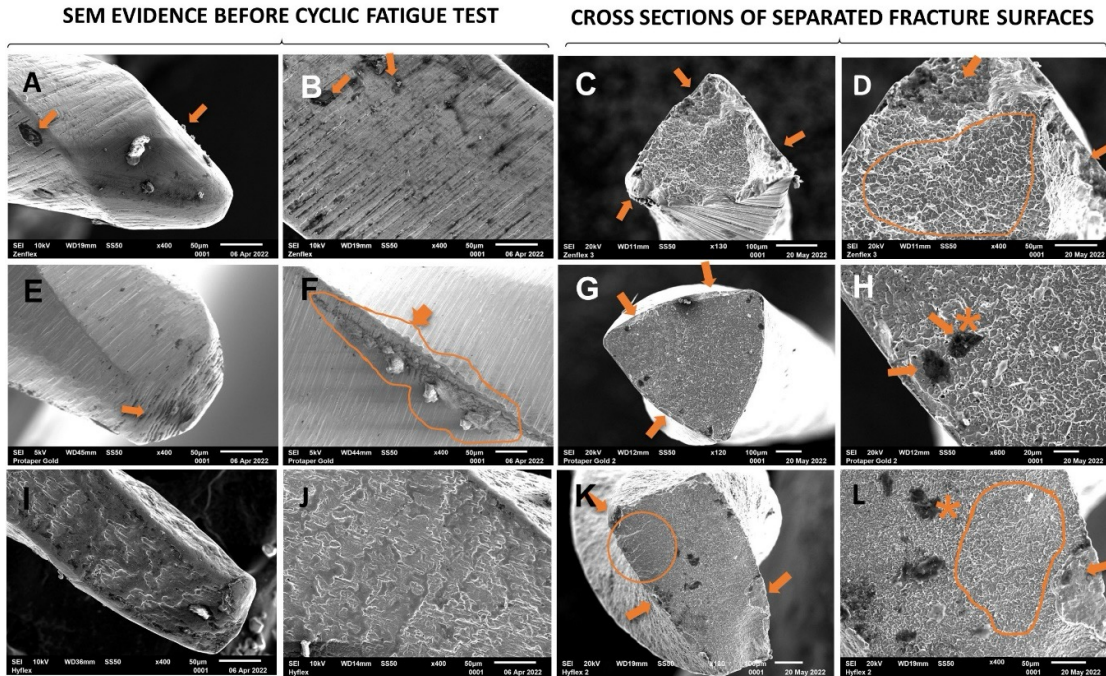


**Figure 2.** Scanning Electron Microscopy (SEM) images of the surface of the new instruments. New ZenFlex™. Tip of the files. Image at 400x: lateral view of the middle third of the active part. A) ZenFlex™, E) Protaper Gold™ and I) Hyflex™. Macrographs at 3500x: close-up of the tip of the instrument. B) ZenFlex™, F) Protaper Gold™ and J) Hyflex™. SEM micrographs of the fractured instruments after cyclic fatigue tests. Cross section views after being subjected to cyclic fatigue: C) ZenFlex™, G) Protaper Gold™ and K) Hyflex™ EDM; D) ZenFlex™, H) Protaper Gold™ and L) Hyflex™ EDM (400x magnification).

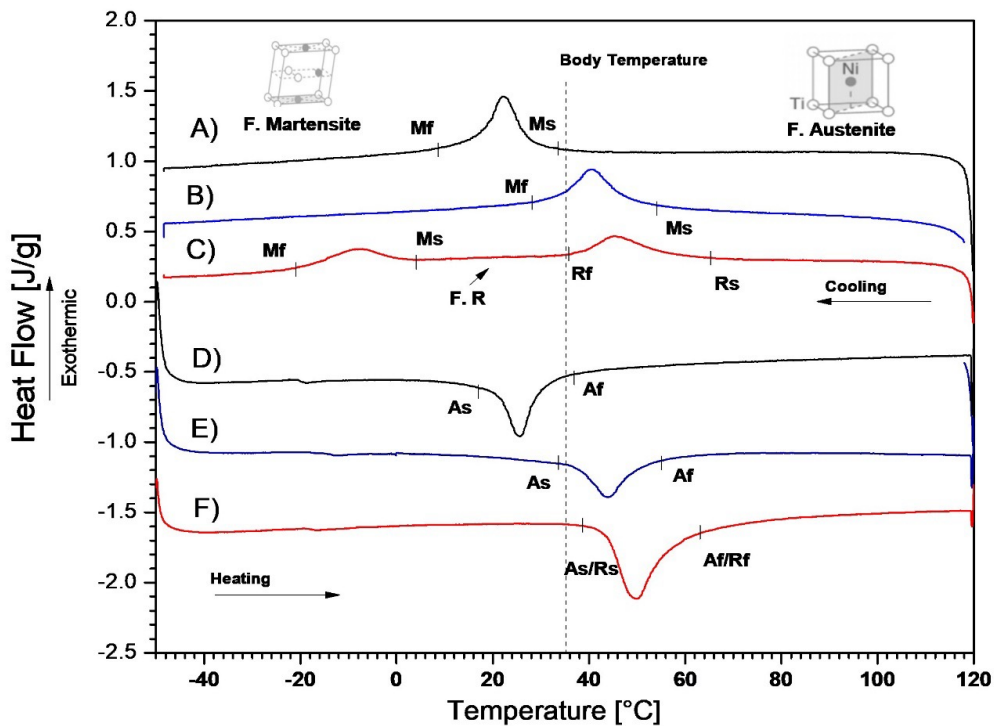


**Figure 3.** DSC thermogram providing information on phase changes in the NiTi alloy of the rotating instruments: Cooling: A) Zenflex™, B) Protaper Gold™ and C) Hyflex™ EDM; Heating: D) Zenflex™, E) Protaper Gold™ and F) Hyflex™ EDM. As= austenitic onset; Af= austenitic finish; Ms= martensitic onset; Mf= martensitic finish; Rs= R-phase onset; Rf= R-phase finish; F. R= R-phase.

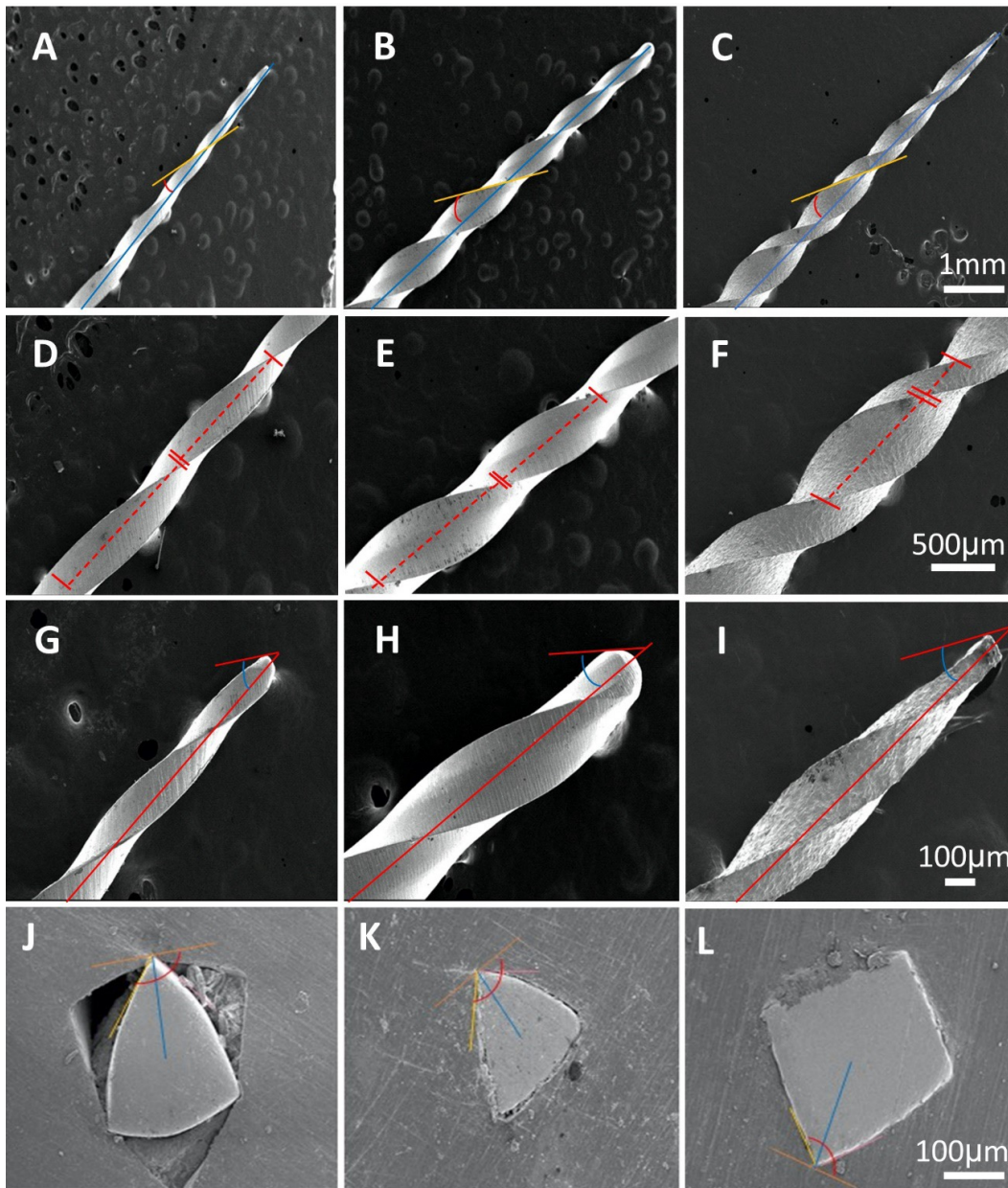


**Figure 4.** Morphological characterization by scanning electron microscopy. Analysis of the helical angle at 25x. A) ZenflexTM, B) Protaper GoldTM, and C) HyflexTM EDM; Pitch analysis at 50x. D) ZenflexTM, E) Protaper GoldTM and F) HyflexTM EDM; Transition angle at 100x. G) ZenflexTM, H) Protaper GoldTM and I) HyflexTM EDM. The rotary instruments feature passive tips, both with a rounded shape for ZenflexTM and Protaper GoldTM, while the HyflexTM EDM features a flat tip; Cutting and tilt angle at 200x. J) ZenflexTM, K) Protaper GoldTM and L) HyflexTM EDM. HyflexTM EDM has a polyhedral section, while ZenflexTM and Protaper GoldTM have a triangular-shaped section.

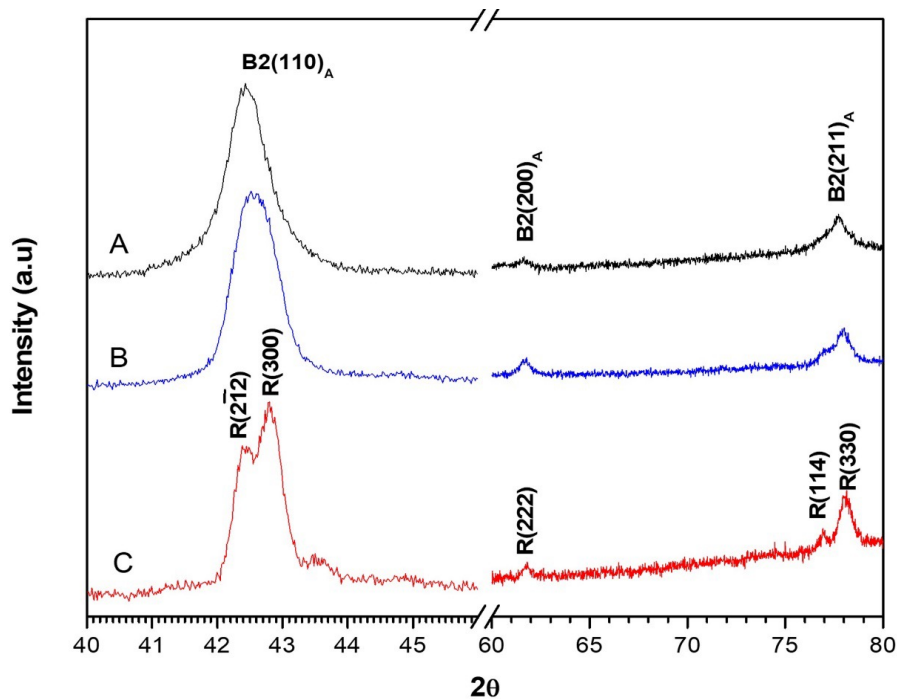


**Figure 5.** X-ray diffraction from rotating A) ZenFlex<sup>TM</sup>, B) Protaper Gold<sup>TM</sup> and C) HyFlex<sup>TM</sup> EDM instruments.

## DISCUSSION

Cyclic fatigue stands as the primary cause of instrument fracture, accounting for between 50 and 90% of mechanical failures (17). This phenomenon is influenced by various factors, including anatomical aspects of the root canal such as radius and angle of curvature, as well as the physical and chemical properties of the NiTi alloy (e.g., equiatomic ratio, heat treatment, and crystallographic arrangement), alongside the design of the instrument and the kinematics of the drive motor (11, 18, 19). It's crucial to recognize that these factors do not act independently; rather, they collectively contribute to instrument fracture.

The objective of this study was to assess the cyclic fatigue fracture of ZenFlex<sup>TM</sup>, Protaper Gold<sup>TM</sup>, and HyFlex<sup>TM</sup> EDM rotary files in simulated curved canals while also examining their physicochemical properties. The absence of regulations governing the marketing of NiTi rotary files without prior studies can lead to accidents during

the endodontic procedure, as operators may be unaware of the mechanical and physical characteristics of the instruments they are working with.

SEM studies have revealed the presence of cracks and defects on the surface of new NiTi instruments, likely associated with manufacturing processes, which can predispose them to fracture and reduce their fatigue resistance. These defects often act as stress concentration points, initiating cracks that propagate to critical lengths, ultimately resulting in fracture (20, 21). This is exemplified by the observation of cracks and defects on the cutting edges of Protaper Gold<sup>TM</sup> and ZenFlex<sup>TM</sup> instruments prior to cyclic fatigue evaluation, which coincide with the fracture sites observed after the cyclic fatigue analysis.

The fractographic study of post-fracture micrographs, combined with findings from existing literature, indicates that patterns of cones and craters of ductile rupture are characteristic features of cyclic fatigue failure. These patterns have

been extensively documented in previous studies (12, 17, 19, 22, 23). During cyclic fatigue failure, cracks initiate and propagate due to the presence of machining imperfections, such as corners and defects, which act as stress concentration points. These imperfections serve as the starting points for fatigue cracks, which then propagate under the alternating tensile-compressive bending stresses experienced during cyclic loading. Even a few larger particles are sufficient to initiate microcavity growth and coalescence without causing macroscopic plastic deformation. As the cracks propagate and coalesce, they result in the formation of a fracture surface characterized by hemispherical depressions, often referred to as cones. This process underscores the importance of understanding the role of surface imperfections and cyclic loading in the fatigue failure of NiTi rotary instruments, as it provides insights into the mechanisms underlying their fracture behavior. According to the findings of the present study, ZenFlex™ files exhibit greater resistance to cyclic fracture, attributed to their lower metallic mass and triangular cross-section. Previous research has demonstrated that instruments with a triangular cross-section, like ZenFlex™, possess greater resistance to cyclic fatigue compared to those with a convex triangular or rectangular cross-section of similar diameter (24-26). Furthermore, instruments with a smaller taper, such as ZenFlex™, demonstrate enhanced resistance to cyclic fatigue compared to larger instruments with greater taper. This is because the size at the point of maximum stress during a test can significantly impact the fatigue life of NiTi rotary instruments (27, 28). However, despite ZenFlex™'s superior performance in terms of cyclic fatigue, HyFlex™ EDM exhibits longer resistance to cyclic fracture. Studies, such as those conducted by Kaval *et al.* (29), recommend using files like HyFlex™ EDM for safe use in highly curved canals due to their increased resistance to bending fatigue. The prolonged resistance to cyclic fracture observed in HyFlex™ EDM may be attributed to the presence of the R

phase in the thermograms, which is characterized by a two-step transformation (austenite to R phase and R phase to martensite) (30). This intermediate phase, positioned between the austenite and martensite phases, contributes to enhancing fatigue life. This enhancement may be associated with dislocation networks and/or coherent precipitations of Ni<sub>4</sub>Ti<sub>3</sub> formed during cooling, which are generated by thermomechanical treatments such as post-deformation annealing (9, 31).

Similarly, it has been observed that the austenitic transformation temperature ( $A_s$ ) commences at 38.4°C, indicating that the HyFlex™ EDM instrument undergoes a transition between the R-martensite phases at the onset of treatment, thereby enhancing its resistance to bending (32). Zenflex is in an austenitic phase, rendering it more rigid, which is associated with a slight increase in the nickel content in the equiatomic ratio of the NiTi alloy, leading to a decrease in the starting temperature of the martensitic state transition ( $M_s$ ) (33). However, Zenflex™ offers two smaller tapers than HyFlex™ EDM, potentially benefiting from cases with more aberrant curvatures. In the case of Protaper Gold™, the transition temperature range is 30-60°C, indicating that the instrument transitions between the austenite and martensite phases at the beginning of treatment, possibly making Protaper Gold™ more reliable in the treatment of narrow and calcified root canals. Additionally, studies have demonstrated the superiority of the HyFlex™ EDM instrument over Protaper Gold™, as files manufactured with controlled memory have been reported to exhibit greater resistance to cyclic fatigue (34, 35).

Regarding the design of rotary instruments, Hyflex™ EDM has a wider angle ( $21.271 \pm 0.73^\circ$ ), which can induce faster dentin wear, thus presenting a greater risk of the instrument becoming lodged in the walls, which can cause a fracture. Concerning the pitch or thread pitch, the Hyflex™ EDM instrument features smaller spaces between spirals or

thread pitches, which decreases the tendency to twist and suction tendencies decrease (36).

The analysis of all the obtained results allows us to discern the advantages conferred by the instruments through a combination of factors, including design, chemical composition, crystallographic structure, and thermal treatments, all of which influence the mechanical properties of the instruments, particularly their resistance to cyclic fatigue. By considering these aspects, clinicians can make informed decisions when selecting the most suitable rotary instrument for each specific case, thereby enhancing treatment safety. Also, it is important to note the absence of an international standard for evaluating the fatigue resistance of rotary instruments, with the American Dental Association (ADA) yet to establish a standardized protocol for testing. Cyclic fatigue tests vary widely in design, making it challenging to compare results across studies. Discrepancies in study findings can also be attributed to differences in endodontic motors, where real kinematic values such as torque and rpm may differ from manufacturers' declared values. Additionally, variations in the devices used for evaluating cyclic fatigue contribute to divergent results. Notably, most research employs static conditions, with only a small percentage utilizing dynamic fatigue devices (13). Static models apply flexion forces consistently at the same point on the file, failing to replicate the real conditions encountered in clinical practice, where files are not stationary within the canals during instrumentation (14). In contrast, dynamic models distribute tension along a broader area along the instrument's axis and mimic the pecking movement performed by clinicians during root canal treatment (11). These dynamic models provide a more realistic simulation of clinical scenarios, offering valuable insights into the fatigue resistance of rotary instruments under dynamic conditions.

The AED utilized in our study offers several key advantages over alternative devices. Notably, its ability to record crucial data such as the number of cycles and fracture time, coupled with automation and self-calibration features, sets it apart (37). One of its most significant advantages lies in its capability to mitigate the influence of human error, ensuring consistent and reliable results. By providing precise control over applied force and speed, the AED proved to be highly effective in evaluating cyclic fracture parameters. Although the standardized stainless-steel artificial canal cannot fully replicate clinical conditions, it serves to minimize extraneous variables influencing file fracture beyond cyclic fatigue (37). Consequently, the findings from these *in vitro* studies hold considerable value for endodontic specialists, offering valuable insights into treatment protocols (29).

Finally, it is important to acknowledge certain limitations inherent in the research. Firstly, the ZenFlex™ files' torsional fracture was not evaluated, nor was their fracture due to cyclic fatigue investigated in an *in vitro* model using extracted teeth. Additionally, the study did not encompass comparisons involving higher degrees of curvature. Addressing these limitations could provide further depth to the understanding of rotary instrument performance and fracture mechanisms. Future studies could further explore the clinical implications of the differences in cyclic fatigue resistance among these NiTi rotary file systems, particularly in challenging clinical scenarios such as retreatments or curved canal anatomies. Investigating the long-term performance of these instruments under dynamic conditions, including repetitive use and sterilization cycles, could provide valuable insights into their durability. Additionally, advanced characterization techniques, may help elucidate the role of heat treatment and crystalline structure on mechanical properties.

## CONCLUSIONS

The ZenFlex™ file demonstrated superior resistance to cyclic fatigue, demonstrating its durability under repetitive stress. Conversely, the HyFlex™ EDM file exhibited prolonged working time prior to fracture, indicating its resilience in withstanding prolonged usage. On the other hand, the Protaper Gold™ file exhibited a larger size of separated fragments upon fracture.

## AUTHOR CONTRIBUTION STATEMENT

Conceptualization and design: M.V.M.G. and M.G.S.

Literature review: M.C.B.J., A.I.O., M.V.M.G. and M.G.S.

Methodology and validation: V.A.E.B., A.P.G., C.G.F. and M.G.S.

Formal analysis: V.A.E.B., A.P.G., M.V.M.G. and M.G.S.

Investigation and data collection: M.C.B.J., A.I.O., C.G.F., A.P.G. and M.G.S.

Resources: V.A.E.B., A.P.G. and M.V.M.G.

Data analysis and interpretation: A.P.G., M.V.M.G. and M.G.S.

Writing-original draft preparation: M.V.M.G. and M.G.S.

Writing-review & editing: A.P.G., C.G.F. and M.G.S.

Supervision: M.V.M.G., A.P.G. and M.G.S.

Project administration: C.G.F., A.P.G. and M.V.M.G.

Funding acquisition: A.P.G. and M.V.M.G.

## ACKNOWLEDGMENTS

María Concepción Betanzos-Juárez and Alejandra Izquierdo-Orozco thank CONAHCYT for the scholarship granted for the master's degree in Endodontics at the UASLP.

## REFERENCES

1. Walia H.M., Brantley W.A., Gerstein H. An initial investigation of the bending and torsional properties of Nitinol root canal files. *J Endod* 1988; 14 (7): 346-51. doi: 10.1016/s0099-2399(88)80196-1. PMID: 3251996.
2. Schäfer E., Schulz-Bongert U., Tulus G. Comparison of hand stainless steel and nickel titanium rotary instrumentation: a clinical study. *J Endod* 2004; 30 (6): 432-5. doi: 10.1097/00004770-200406000-00014. PMID: 15167474.
3. Esposito P.T., Cunningham C.J. A comparison of canal preparation with nickel-titanium and stainless steel instruments. *J Endod* 1995; 21 (4): 173-6. doi: 10.1016/S0099-2399(06)80560-1. PMID: 7673815.
4. Himel V.T., Ahmed K.M., Wood D.M., Alhadainy H.A. An evaluation of nitinol and stainless steel files used by dental students during a laboratory proficiency exam. *Oral Surg Oral Med Oral Pathol Oral Radiol Endod* 1995; 79 (2): 232-7. doi: 10.1016/s1079-2104(05)80289-6. PMID: 7614188.
5. Ashkar I., Sanz J.L., Forner L. Cyclic Fatigue Resistance of Glide Path Rotary Files: A Systematic Review of in Vitro Studies. *Materials (Basel)* 2022; 15 (19): 6662. doi: 10.3390/ma15196662. PMID: 36234003; PMCID: PMC9571085.
6. Świec P., Zubko M., Stróż D., Lekston Z. Martensitic transformation in nanostructured NiTi alloy studied by X-ray diffraction in-situ heating. *Mater Trans* 2019; 60 (5). <https://doi.org/10.2320/matertrans.MC201808>.
7. Honarvar M., Konh B., Podder T.K., Dicker A.P., Yu Y., Hutapea P. X-ray Diffraction Investigations of Shape Memory NiTi Wire.

- J Mater Eng Perform 2015; 24 (8). doi: 10.1007/s11665-015-1574-2
8. Santos Lde A., Resende P.D., Bahia M.G., Buono V.T. Effects of R-Phase on Mechanical Responses of a Nickel-Titanium Endodontic Instrument: Structural Characterization and Finite Element Analysis. *ScientificWorldJournal* 2016; 7617493. doi: 10.1155/2016/7617493. Epub 2016 May 22. PMID: 27314059; PMCID: PMC4893430.
  9. Wang X.B., Verlinden B., Van Humbeeck J. R-phase transformation in NiTi alloys. *Materials Science and Technology (United Kingdom)* 2014; 30 (13): 1517-29. doi:10.1179/1743284714Y.00000000590
  10. Zhu J., Wu H.H., Wu Y., Wang H., Zhang T., Xiao H., et al. Influence of Ni<sub>4</sub>Ti<sub>3</sub> precipitation on martensitic transformations in NiTi shape memory alloy: R phase transformation. *Acta Mater.* 2021; 207 (February): 116665. doi.org/10.1016/j.actamat.2021.116665
  11. Ruiz-Sánchez C., Faus-Llácer V., Faus-Matoses I., Zubizarreta-Macho Á., Sauro S., Faus-Matoses V. The Influence of NiTi Alloy on the Cyclic Fatigue Resistance of Endodontic Files. *J Clin Med* 2020; 9 (11): 3755. doi: 10.3390/jcm9113755. PMID: 33233442; PMCID: PMC7700305.
  12. Lo Savio F., La Rosa G., Bonfanti M., Alizzio D., Rapisarda E., Pedullà E. Novel Cyclic Fatigue Testing Machine for Endodontic Files. *Exp Tech* 2020; 44 (5). doi.org/10.1016/j.joen.2011.09.028
  13. Hülsmann M., Donnermeyer D., Schäfer E. A critical appraisal of studies on cyclic fatigue resistance of engine-driven endodontic instruments. *Int Endod J* 2019; 52 (10): 1427-1445. doi: 10.1111/iej.13182. Epub 2019 Jul 25. PMID: 31267579.
  14. Ferreira F., Adeodato C., Barbosa I., Aboud L., Scelza P., Zaccaro Scelza M. Movement kinematics and cyclic fatigue of NiTi rotary instruments: a systematic review. *Int Endod J* 2017; 50 (2): 143-52. doi: 10.1111/iej.12613. Epub 2016 Feb 26. PMID: 26825427.
  15. Martins J.N.R., Silva E.J.N.L., Marques D., Ajuz N., Rito Pereira M., Pereira da Costa R., Braz Fernandes F.M., Versiani M.A. Characterization of the file-specific heat-treated ProTaper Ultimate rotary system. *Int Endod J* 2023; 56 (4): 530-542. doi: 10.1111/iej.13880. Epub 2022 Dec 21. PMID: 36508297.
  16. Gaitán-Fonseca C., Lara-Alvarado E., Flores-Reyes H., Pozos-Guillén A., Méndez-González V. Automatic Electronic Device Used for the Evaluation of Cyclic-Fatigue Resistance of Nickel-Titanium Instruments. *Odovtos - International Journal of Dental Sciences* 2017; 19 (1). doi.org/10.15517/ijds.v19i1.27288
  17. Pedullà E., Lo Savio F., Boninelli S., Plotino G., Grande N.M., Rapisarda E., La Rosa G. Influence of cyclic torsional preloading on cyclic fatigue resistance of nickel - titanium instruments. *Int Endod J* 2015; 48 (11): 1043-50. doi: 10.1111/iej.12400. Epub 2014 Nov 18. PMID: 25353957.
  18. Ruiz-Sánchez C., Faus-Matoses V., Alegredomingo T., Faus-Matoses I., Faus-Llácer V.J. An in vitro cyclic fatigue resistance comparison of conventional and new generation nickel-titanium rotary files. *J Clin Exp Dent* 2018;10(8):e805-e809. doi: 10.4317/jced.55091. PMID: 30305880; PMCID: PMC6174015.
  19. Uygun A.D., Kol E., Topcu M.K., Seckin F., Ersoy I., Tanriver M. Variations in cyclic fatigue resistance among ProTaper Gold, ProTaper Next and ProTaper Universal instruments at different levels. *Int Endod J* 2016; 49 (5): 494-9. doi: 10.1111/iej.12471. Epub 2015 Jun 5. PMID: 26011308.
  20. Tripi T.R., Bonaccorso A., Condorelli G.G. Cyclic fatigue of different nickel-titanium endodontic rotary instruments. *Oral Surg Oral Med Oral Pathol Oral Radiol Endod*

- 2006; 102 (4): e106-14. doi: 10.1016/j.tripleo.2005.12.012. Epub 2006 Jul 14. PMID: 16997084.
21. Lopes H.P., Elias C.N., Vieira M.V., Vieira V.T., de Souza L.C., Dos Santos A.L. Influence of Surface Roughness on the Fatigue Life of Nickel-Titanium Rotary Endodontic Instruments. *J Endod* 2016; 42 (6): 965-8. doi: 10.1016/j.joen.2016.03.001. Epub 2016 Apr 12. PMID: 27080117.
  22. Uygun A.D., Unal M., Falakaloglu S., Guven Y. Comparison of the cyclic fatigue resistance of hyflex EDM, vortex blue, protaper gold, and onecurve nickel-Titanium instruments. *Niger J Clin Pract* 2020; 23 (1): 41-45. doi: 10.4103/njcp.njcp\_343\_19. PMID: 31929205.
  23. Gündoğar M., Özyürek T. Cyclic Fatigue Resistance of OneShape, HyFlex EDM, WaveOne Gold, and Reciproc Blue Nickel-titanium Instruments. *J Endod* 2017; 43 (7): 1192-1196. doi: 10.1016/j.joen.2017.03.009. Epub 2017 May 17. PMID: 28527845.
  24. Cheung G.S., Zhang E.W., Zheng Y.F. A numerical method for predicting the bending fatigue life of NiTi and stainless steel root canal instruments. *Int Endod J* 2011; 44 (4): 357-61. doi: 10.1111/j.1365-2591.2010.01838.x. Epub 2011 Jan 10. PMID: 21219364.
  25. Capar I.D., Kaval M.E., Ertas H., Sen B.H. Comparison of the cyclic fatigue resistance of 5 different rotary pathfinding instruments made of conventional nickel-titanium wire, M-wire, and controlled memory wire. *J Endod* 2015; 41 (4): 535-8. doi: 10.1016/j.joen.2014.11.008. Epub 2014 Dec 12. PMID: 25510316.
  26. Ruiz-Sánchez C., Faus-Matoses V., Alegre-Domingo T., Faus-Matoses I., Faus-Llacer V.J. An in vitro cyclic fatigue resistance comparison of conventional and new generation nickel-titanium rotary files. *J Clin Exp Dent* 2018; 10 (8): e805-e809. doi: 10.4317/jced.55091. PMID: 30305880; PMCID: PMC6174015.
  27. Zupanc J., Vahdat-Pajouh N., Schäfer E. New thermomechanically treated NiTi alloys - a review. *Int Endod J* 2018; 51 (10):1088-1103. doi: 10.1111/iej.12924. Epub 2018 Apr 19. PMID: 29574784.
  28. Uygun A.D., Unal M., Falakaloglu S., Guven Y. Comparison of the cyclic fatigue resistance of hyflex EDM, vortex blue, protaper gold, and onecurve nickel-Titanium instruments. *Niger J Clin Pract* 2020; 23 (1): 41-5. doi: 10.4103/njcp.njcp\_343\_19. PMID: 31929205.
  29. Kaval M.E., Capar I.D., Ertas H. Evaluation of the Cyclic Fatigue and Torsional Resistance of Novel Nickel-Titanium Rotary Files with Various Alloy Properties. *J Endod* 2016; 42 (12): 1840-3. doi: 10.1016/j.joen.2016.07.015. Epub 2016 Oct 21. PMID: 27776878.
  30. Zanza A., Seracchiani M., Reda R., Miccoli G., Testarelli L., Di Nardo D. Metallurgical Tests in Endodontics: A Narrative Review. *Bioengineering (Basel)* 2022; 9 (1): 30. doi: 10.3390/bioengineering9010030. PMID: 35049739; PMCID: PMC8773015.
  31. Wang X., Kustov S., Verlinden B., Van Humbeeck J. Fundamental Development on Utilizing the R-phase Transformation in NiTi Shape Memory Alloys. *Shape Memory and Superelasticity* 2015; 1 (2). doi:10.1007/s40830-015-0007-2
  32. Zanza A., Russo P., Reda R., Di Matteo P., Donfrancesco O., Ausiello P., Testarelli L. Mechanical and Metallurgical Evaluation of 3 Different Nickel-Titanium Rotary Instruments: An In Vitro and In Laboratory Study. *Bioengineering (Basel)* 2022; 9 (5): 221. doi:

- 10.3390/bioengineering9050221. PMID: 35621499; PMCID: PMC9137481.
33. Frenzel J., George E.P., Dlouhy A., Somsen C., Wagner M.F.X., Eggeler G. Influence of Ni on martensitic phase transformations in NiTi shape memory alloys. *Acta Mater.* 2010 May; 58 (9): 3444-58. doi.org/10.1016/j.actamat.2010.02.019
34. Capar I.D., Ertas H., Arslan H. Comparison of cyclic fatigue resistance of novel nickel-titanium rotary instruments. *Aust Endod J* 2015; 41 (1): 24-8. doi: 10.1111/aej.12067. Epub 2014 Apr 2. PMID: 24697976.
35. Thu M., Ebihara A., Maki K., Miki N., Okiji T. Cyclic Fatigue Resistance of Rotary and Reciprocating Nickel-Titanium Instruments Subjected to Static and Dynamic Tests. *J Endod* 2020; 46 (11): 1752-1757. doi: 10.1016/j.joen.2020.08.006. Epub 2020 Aug 17. PMID: 32818563.
36. Pedullà E., Lo Savio F., Boninelli S., Plotino G., Grande N.M., La Rosa G, Rapisarda E. Torsional and Cyclic Fatigue Resistance of a New Nickel-Titanium Instrument Manufactured by Electrical Discharge Machining. *J Endod* 2016; 42 (1): 156-9. doi: 10.1016/j.joen.2015.10.004. Epub 2015 Nov 14. PMID: 26586518.
37. Gündoğar M., Özyürek T. Cyclic Fatigue Resistance of OneShape, HyFlex EDM, WaveOne Gold, and Reciproc Blue Nickel-titanium Instruments. *J Endod* 2017; 43 (7): 1192-6. doi: 10.1016/j.joen.2017.03.009. Epub 2017 May 17. PMID: 28527845.